Pairing, temperature, and deformed-shell effects on the properties of superdeformed ^{152}Dy nucleus

J. Dudek
Joint Institute for Heavy Ion Research, Oak Ridge, Tennessee 37831
and Centre de Recherches Nucléaires et Université Louis Pasteur, F-67037 Strasbourg Cedex, France

B. Herskind
The Niels Bohr Institute, DK-4000 Roskilde, Denmark

W. Nazarewicz
Institute of Physics, Technical University, PL-00-662 Warsaw, Poland

Z. Szymanski and T. R. Werner
Centre de Recherches Nucléaires, F-67037, Strasbourg Cedex, France
and Institute of Theoretical Physics, Warsaw University, PL-00-681 Warsaw, Poland
(Received 8 February 1988)

The existence of superdeformed shell closures together with pairing and the nuclear temperature effects are shown to explain the originally unexpected properties of the superdeformed band observed up to $I \sim 60\hbar$ in the ^{152}Dy nucleus. No parameters were adjusted to the superdeformed band properties. Population, and depopulation of the superdeformed bands, the moments of inertia, and side feeding properties are discussed and qualitatively understood. The use of the free-energy calculation results and the microcanonical ensemble formulation of the level-density problem at high-spin are proposed and discussed.

I. INTRODUCTION

The recent explosion of interest in high-spin behavior of strongly elongated (superdeformed) nuclei is well justified by the very special nature of those states. The presence of exotic intruder orbitals under the Fermi level, the very large $E2$ transition rates of about 2500 WU or more, the relatively unusual conditions for charged-particle emission due to the drastically lowered Coulomb barriers, these are only a few examples of the extreme microscopic mechanisms inducing "unusual" behavior.

The superdeformed shapes whose existence was predicted first by theory have been observed recently in experiments. They are the manifestations of strong, "deformed shell" effects, which remain in close analogy to the well-known spherical shell closures of Goeppert-Mayer and Jensen. The present study has been motivated primarily by the new experimental results on $^{152}_{66}Dy_{86}$ nucleus.

The high-spin properties of $^{152}_{66}Dy_{86}$ have been extensively studied in the past mainly because of the pronounced isomerism characteristic of a noncollective rotation. Competing collective decay modes have been established[1,2] relatively late and only recently a regular γ-decay sequence[3] with properties characteristic[4] of the superdeformed structure has been reported. Discovery of the corresponding rotational band extending up to spin $I \sim 60\hbar$ showed simultaneously several *a priori unexpected* features: (a) The constant angular momentum gain $I \simeq \text{const}\omega$ (ω=rotational frequency); (b) significant concentration of the population on one superdeformed band; (c) very small side-feeding for most of the superdeformed states at $I \leq 56\hbar$; and (d) the rapid depopulation of the superdeformed band over about three transitions around spin $I \sim 26\hbar$.

In this article we discuss the possible influence of the *nuclear shell and pairing correlations and thermal excitations* on the above features. (Discussion of details related to a competition between triaxial and superdeformed shape configurations[5,6] or of the predicted band structure[7,8] can be found in literature.)

In obtaining the results presented below several well-established techniques were employed and this is likely to reduce the uncertainties related to a possible model dependence of the final result. In calculating total nuclear energy, the Woods-Saxon average field[9] and cranking approximation[7,9] have been used. The pairing effect was accounted for using the independent quasiparticle approximation, and the so-called particle-number projection technique, Ref. 10. Thermal excitations were treated using the concept of free energy, calculated as in Ref. 11. (An overview of the applied techniques can be found in Ref. 12; modifications are discussed below.)

In Sec. II the shape evolution and coexistence between "normally"- and "super"-deformed states are discussed taking into account the effect of thermal excitation. This discussion addresses in particular the disappearance of the potential barriers which separate the superdeformed minima from the rest of the total energy landscape.

Section III presents the results of the "full-scale" (β_2,γ,β_4) energy minimization in the presence of the pairing interactions. The highest-spin limit is discussed in particular and a comparison with experiment illustrated. Characteristic global features of the population

 ©1988 The American Physical Society

(nonzero temperatures) and depopulation (zero temperature limit) of the superdeformed band in ^{152}Dy are discussed in Sec. IV. In particular, the level density calculations are presented. The results are summarized in Sec. V.

II. SHAPE EVOLUTION EFFECTS IN THE PRESENCE OF THERMAL EXCITATIONS

An effective method of calculating the nuclear shape properties in function of global parameters such as, for instance, deformation β (here one symbol stands for several shape degrees of freedom, e.g., $\beta_2,\gamma,\beta_4,\ldots$) rotational frequency ω, nuclear temperature T, etc., is provided by Strutinsky's macroscopic-microscopic method. Since Strutinsky's approach in its various particular cases has been in use for many years, only those aspects are given here which are necessary for the unique definition of our final result.

The total energy formula involves, as usual, a splitting into macroscopic and microscopic terms, the latter generated using the deformed Woods-Saxon potential.[13] Having solved the Schrödinger equation (with the so-called Woods-Saxon universal parameter set as defined in Ref. 13)

$$H_{\rm WS}\psi_\nu = e_\nu \psi_\nu \tag{1a}$$

or, for a rotating nucleus, the analogous, so-called cranking equation

$$H^\omega \psi_\nu^\omega = e_\nu^\omega \psi_\nu^\omega, \quad H^\omega = H_{\rm WS} - \omega j_x \ , \tag{1b}$$

one calculates the total energy of a nucleus in a rotating coordinate frame (the Routhian) as

$$R^\omega({\rm def}) = E^{\omega=0}_{\rm macro}({\rm def}) + E^{\omega=0}_{\rm micro}({\rm def}) + \sum_{\nu\ {\rm occ}} [e_\nu^\omega({\rm def}) - e_\nu^{\omega=0}({\rm def})] \ , \tag{2}$$

with the summation extending over all occupied levels. Here, the macroscopic term $E^{\omega=0}_{\rm macro}({\rm def})$ is calculated as in Ref. 14 and $E^{\omega=0}_{\rm micro}({\rm def})$ as in Ref. 15, with the smoothing order $p=6$ and smoothing range $\gamma = 1.2\hbar\omega_0$ ($\hbar\omega_0 = 41/A^{1/3}$ MeV); for definitions and notation cf., e.g., Ref. 15. Expression (2) applies in this form for the Woods-Saxon type potentials (Woods-Saxon, folded Yukawa) as discussed, e.g., in Ref. 12; in this respect the Nilsson model potential requires special care, Ref. 16. The detailed relations between the two average field approaches are discussed in Ref. 17.

If necessary a transformation between the rotating and the laboratory coordinate frames can be obtained in a usual manner (see, e.g., Ref. 10), leading to

$$E(I,{\rm def}) = R^\omega({\rm def}) + \omega I, \quad I = \sum_{\nu\ {\rm occ}} (j_x)_{\nu\nu} \ , \tag{3}$$

an equivalent energy representation in the laboratory system of reference. This kind of representation will be used in Figs. 1–3.

Our calculations of the total energy surfaces in function of the quadrupole (β_2,γ) deformations give, in agreement with experimental results, a coexistence between the oblate-shape noncollective, triaxial, and superdeformed collective equilibrium deformations. The corresponding overview of the total energy landscapes obtained using the Woods-Saxon deformed single-particle potential is shown in Fig. 1 for a number of increasing spin values. Here the pairing, whose effects will be treated separately below, was neglected. This part of the calculation has been performed taking into account an effect of the hexadecapole deformation in a simplified manner. At each (β_2,γ) point the β_4 value has been fixed after minimizing the total *classical* energy at a fixed spin value $I=I_0$. We selected $I_0=40$ in order to optimize the results to some extent for both the very high (up to $I\sim 60$) and the moderate ($I\sim 20$) spin limits. By doing so the possibility of a systematic large error due to β_4 effect on the total energy result is to a far extent reduced. (The final results compared to experiment in Sec. III will contain both the effect of pairing and full β_4 minimization.)

The results in Fig. 1 show that the moderate-deformation minima; $\gamma=60°$, oblate shape with spin parallel to the symmetry axis, and the triaxial one are clearly *evolving when spin increases.* On the contrary, the superdeformed minimum *remains considerably stable* with respect to increasing rotation (cf. also Ref. 7).

To gain some insight into the shape coexistence problem when the nuclear temperature is different from zero, i.e., at the conditions met when the corresponding states are populated in heavy-ion reactions, calculations have been performed assuming a thermal equilibrium situation at each (β_2,γ) point. Calculations of this type involve as usual the free-energy in the rotating coordinate frame

$$F^\omega({\rm def},T) = R^\omega({\rm def},T) - TS^\omega({\rm def},T) \tag{4}$$

as the adequate thermodynamical potential to describe a nuclear object after its thermal equilibration. The entropy is calculated from the standard expression

$$S^\omega({\rm def},T) = -\sum_\nu n_\nu^\omega \ln n_\nu^\omega - \sum_\nu (1-n_\nu^\omega)\ln(1-n_\nu^\omega) \tag{5}$$

with the coefficients determining probabilities for the nucleonic levels e_ν^ω to be occupied

$$n_\nu^\omega \equiv n_\nu^\omega({\rm def},T) = \frac{1}{1+\exp\{[e_\nu^\omega({\rm def})-\lambda]/T\}} \ , \tag{6}$$

and where λ, calculated separately for protons and neutrons, satisfies

$$(N \text{ or } Z) = \sum_{\nu\ {\rm occ}} n_\nu^\omega({\rm def},T) \ . \tag{7}$$

For "heated" rotating nuclei one obtains the following generalized Strutinsky method result (see, e.g., Refs. 11 and 18):

$$R^\omega({\rm def},T) = R^\omega({\rm def},T=0) + U^\omega({\rm def},T) \tag{8}$$

with the microscopic thermal excitation energy defined, as usual, by

$$U^\omega({\rm def},T) = \sum_\nu n_\nu^\omega({\rm def},T) e_\nu^\omega({\rm def}) - \sum_\nu n_\nu^\omega({\rm def},T=0) e_\nu^\omega({\rm def}) \ . \tag{9}$$

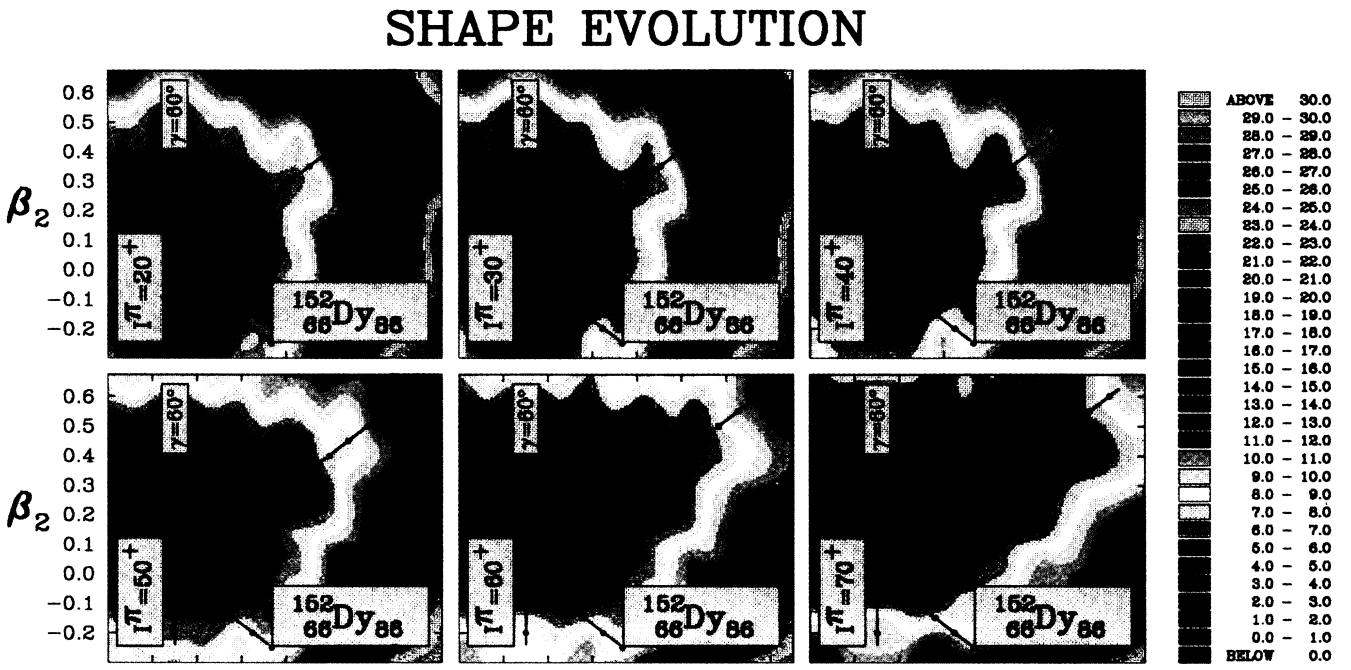

FIG. 1. The total energy surfaces in the (β_2,γ) plane with the $\beta_4=\beta_4(\beta_2,\gamma)$ optimized, as discussed in text. The convention related to the sign of the triaxiality parameter γ is as follows: $\gamma=60°$ corresponds to oblate shape noncollective rotation with spin parallel to the symmetry axis, $\gamma=0°$ (nearly diagonal axis) corresponds to collective rotation of the prolate deformed nucleus with the symmetry axis perpendicular to spin, etc. The lowest energy minima are marked with dark blue in the landscapes and the color scale defines the energy elevation (in MeV).

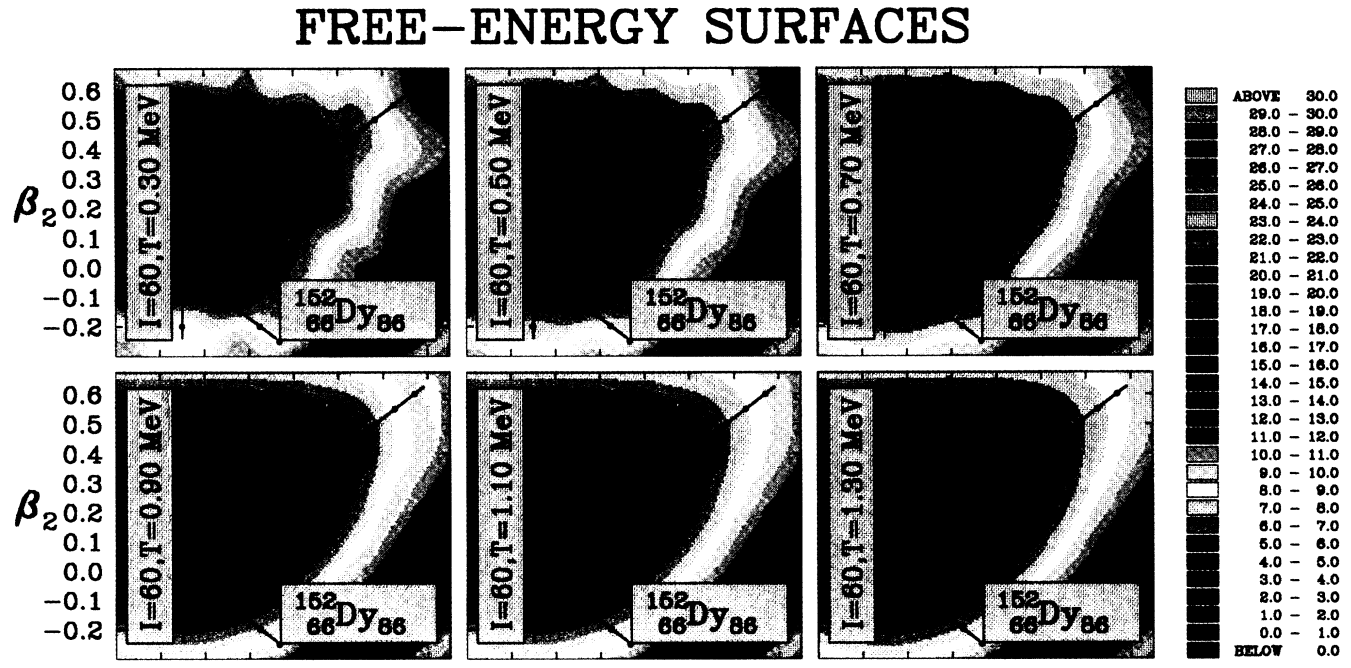

FIG. 2. The total free-energy surfaces calculated as discussed in text for $I=60$. Various frames correspond to increasing temperature. Note the early disappearance of the shell structure responsible for various coexisting minima already at $T\sim 800$ keV. The definition of the coordinate system is the same as in Fig. 1.

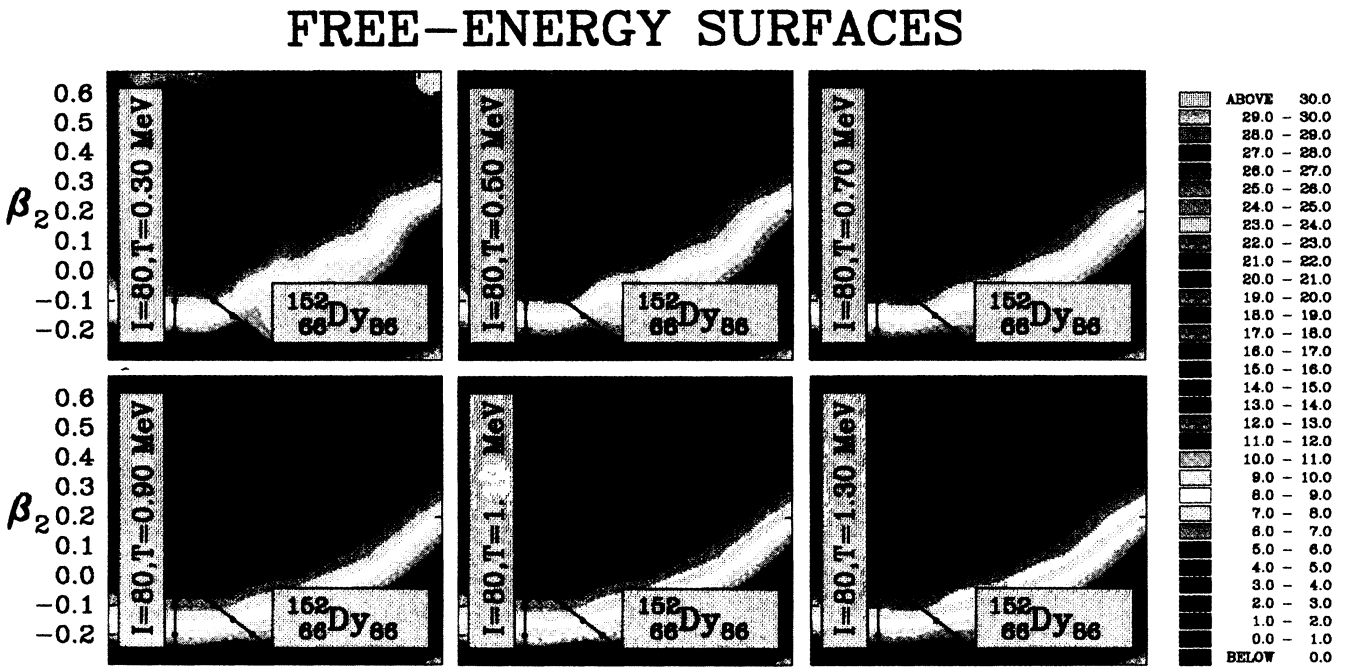

FIG. 3. Similar to Fig. 2 but at $I=80$, i.e., close to the so-called Jacobi instability (for more details see captions to Figs. 1 and 2). Note that disappearance of the shell structure responsible for various minima affects the barrier height considerably.

The temperature effect on the macroscopic energy term in Eq. (2) can be considered neglegible in the temperature range of interest here ($T \leq 2$ MeV) (cf., e.g., Diebel *et al.*,[19] and references therein).

Transformation (3) can be applied to Eq. (4) as well with

$$I = \sum_{\nu} n_{\nu}^{\omega(I)}(\mathrm{def}, T)(j_x)_{\nu\nu} \ . \tag{10}$$

The results of Eq. (4) have been often represented in terms of the free-energy landscapes over the (β_2, γ) plane. Before discussing further the meaning of such a representation and its possible modifications (in Sec. IV) let us illustrate the characteristic evolution in the normal versus superdeformed shape coexistence picture when temperature increases. Such an illustration is given in Figs. 2 and 3 where the free-energy surfaces at spins $I=60$ and 80, respectively, are represented for temperatures $T=0.3$, 0.7, 1.1, 1.5, 1.9, and 2.3 MeV. From Fig. 2 it becomes clear that at spins $I \sim 60$ "heating up" the ^{152}Dy nucleus to $T \sim (0.8$ to $0.9)$ MeV should result in a disappearance of the shell effects responsible for identification of a well-defined superdeformed minimum. Similar results hold for many landscapes at lower and also higher spins.

A slightly exceptional picture applies, however, for a relatively narrow spin range, $\Delta I \sim 6$, at spins close to the so-called Jacobi instability critical spin I_{crit}. It is well known (the particular case of Jacobi instability effect in ^{152}Dy has been treated in Ref. 20) that increasing rotation in classical objects like stars, macroscopic liquid drops, or "nuclear liquid drops" results in a gradual building up of a pronounced oblate shape deformation. Only for $I > I_{\mathrm{crit}}$ a triaxial shape equilibrium develops. These triaxial configurations lose stability against fission already after a relatively small further spin increase. In ^{152}Dy the estimates of Ref. 20 based on the extended nuclear liquid drop model[14] give $I=78$, 80, and 82 as the characteristic spin range over which the triaxial shape configurations evolve fast, leading to fission. It is therefore the narrow spin range around $I \sim I_{\mathrm{crit}}$ where increasing the nuclear temperature removes the barrier separating the super- and the normal-deformed minima but at the same time the free-energy landscape remains flat over a broad deformation range, including superdeformation. (Strictly speaking, the superdeformation even increases with temperature at $I \approx 80$, Fig. 3.) Thus despite the fact that the barrier disappeared, the probability of populating the largely elongated nuclear configurations increases (as discussed in detail in Sec. IV) or at least remains comparable to that of populating moderately deformed states.

III. COEXISTENCE BETWEEN SUPERDEFORMED AND NORMAL DEFORMED SHAPES AND THE EFFECT OF PAIRING

The effects of pairing in the potential energy calculations can be taken into account using the following generalized Strutinsky expression [cf. appendix section in Ref. 12 and compare with Eq. (2)]:

$$R^{\omega}(\mathrm{def}) = E_{\mathrm{macro}}^{\omega=0}(\mathrm{def}) + E_{\mathrm{micro}}^{\omega=0}(\mathrm{def}) + E_{\mathrm{pair}}^{\omega=0}(\mathrm{def}) + [\langle H^{\omega}(\mathrm{def})\rangle_{\mathrm{HFBC}} - \langle H^{\omega=0}(\mathrm{def})\rangle_{\mathrm{HFBC}}] \tag{11}$$

with

$$H^{\omega}=H_{\rm WS}+H_{\rm pair}-\omega j_x \ . \tag{12}$$

[Equation (2) is a particular case of the above expression for vanishing pairing interaction.] We use the monopole pairing Hamiltonian

$$H_{\rm pair}=-G\sum_{\nu\nu'} a^{+}_{\nu}a^{+}_{\bar{\nu}}a_{\bar{\nu}'}a_{\nu'} \ . \tag{13}$$

$E^{\omega=0}_{\rm pair}({\rm def})$ in (11) denotes the usual pairing energy term calculated within the standard BCS approximation. For convenience expression (11) has been "symmetrized" in such a way that the square brackets enclose the rotational contribution normalized to zero at $\omega=0$, and by definition $E^{\omega=0}_{\rm pair}({\rm def})=\langle H^{\omega=0}({\rm def})\rangle_{\rm HFBC}$. The subscript HFBC refers to the traditionally applied name of this approximate approach: the Hartree-Fock-Bogolyubov cranking method. (Details and definitions can be found in Ref. 10; at $\omega=0$ both, i.e., HFBC and BCS methods, coincide.)

Calculation of $\langle H^{\omega}({\rm def})\rangle_{\rm HFBC}$ involves an iterative process to achieve the self-consistency (see, e.g., Ref. 10) and, therefore, is relatively time consuming. For this reason, instead of performing the iterations for all deformation points considered (cf. Figs. 1–3) a limited scale algorithm bringing essentially the same physical information has been applied.

A. Effect of pairing—results of the calculations

Calculations with pairing have been repeated in the vicinities of the total energy minima (see Fig. 1) large enough to allow for the energy minimization with respect to deformation. The minimization over (β_2,γ,β_4) performed independently at each spin shows that the superdeformed minimum is very stable, while the triaxial one evolves with increasing spin. This result confirms the one obtained without pairing correlations, as discussed in Sec. II. The characteristic deformations are given in Fig. 4 where the results of the cranking model calculations for $I=I(\omega)$ dependence (angular momentum gain) are compared to the experimental data.

In the calculations for the superdeformed configurations, a very smooth $I=I(\omega)$ dependence follows from the fact that the deformed-shell closures at $Z=66$ ($\Delta E_{\pi}\sim 0.8$ MeV) and $N=86$ ($\Delta E_{\nu}\sim 1.2$ MeV) are not modified by rotation in any significant way up to the highest spins considered. This stability of the deformed-shell closures follows, in turn, from the fact that in ^{152}Dy the alignment-sensitive single-particle orbitals (e.g., those with small m_j and high-j content) are sufficiently far from the Fermi energies. Another important mechanism very likely to contribute to the "straightening" the I vs ω relation in a superdeformed minimum (as compared to typically more complex I vs ω relations in the moderately deformed nuclei, cf. also the left-hand-side part of Fig. 4) is due to the so-called rotation-deformation scaling. This has to do with the rotation-induced evolution of the overlaps between the relevant single-nucleonic orbitals (cf. Sec. III B and Ref. 21). The latter are responsible in particular for the intensity of pairing correlations in a rotating nucleus and thus to some extent,[21] for details in the angular momentum alignment process.

Taking into account that none of the parameters of the

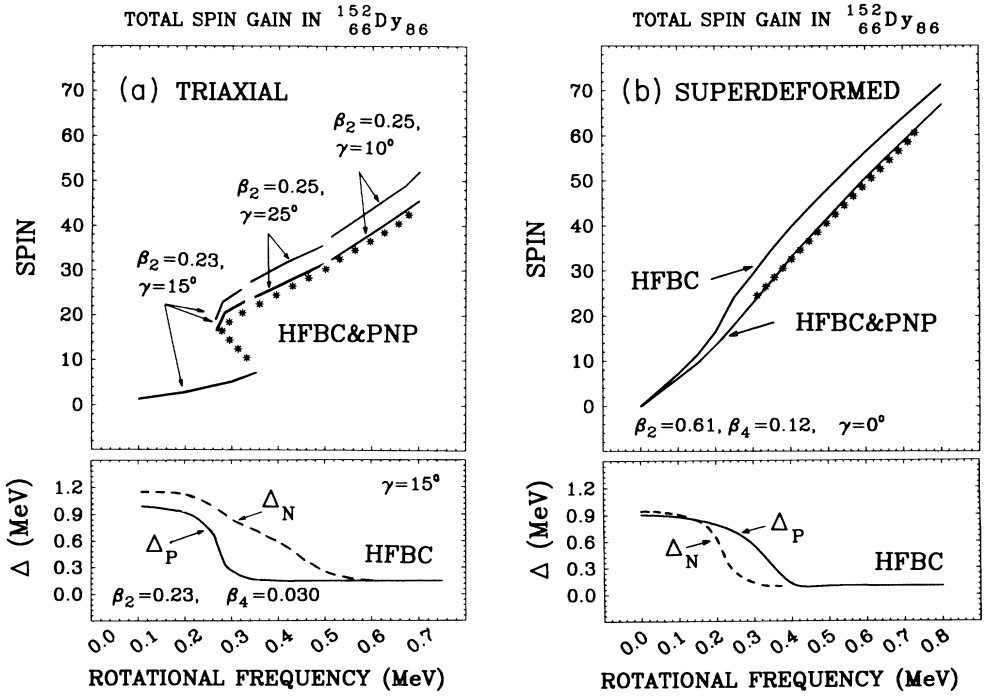

FIG. 4. The spin-gain representation (I vs rotational frequency ω) for the triaxial (left) and superdeformed (right) configurations. The bottom part illustrates the variation of the pairing self-consistent energy gaps according to the HFBC method. Results for the particle number projection variant of the method and the experimental results (asterisks) are also given.

calculation has been fitted to any property of the ^{152}Dy, the agreement between the theoretical and experimental results is remarkable. Slight discrepancies between the two are most likely due to the fact that the multipolarities different than $\lambda=2$ and 4 in the shape parametrizations have been neglected. Also a possibility of, e.g., particle-vibration or other couplings may influence the angular momentum gain to some extent. Including such effects goes, however, beyond the scope of the present study.

The importance of the pairing correlations at the highest spins observed is visible from Fig. 4, where the standard treatment of pairing (HFBC) and the improved one, HFBC with particle number projection (PNP), are compared (for details see Ref. 10). An overestimate as compared to the experiment, in the angular momentum gain by typically $(6-8)\hbar$ when the "static" pairing gaps calculated within HFBC approximation drop to zero (cf. Fig. 4, bottom) reduces practically to zero as compared to experiment after applying the improved (HFBC-PNP) approach with the standard parameters choice. (We use the standard parametrization of pairing, Ref. 22, and the corresponding cutoff which allows for, typically, 50 states distributed symmetrically around the Fermi level.)

According to the theoretical result even at the highest spins considered the pairing correlations are responsible for "dealigning" the angular momentum of $\Delta I \simeq 8\hbar$, as compared to rigid rotation in the superdeformed state.

B. Effects of pairing—discussion

Both formal and physical meaning of the results in Sec. III A can be illuminated using as a guidance some results of the previous studies on the soluble models. Those have been performed by making use of the Hamiltonian formally identical to the one employed in our realistic calculations. The only difference lies in the replacement of the Woods-Saxon single-particle term in Eq. (12) by the corresponding simplified two-level model term. When using the simplified cranking model Hamiltonian

$$H^{\omega}_{\text{soluble}} = H_{\text{SP}} + H_{\text{pair}} - \omega j_x \ , \tag{14}$$

with H_{SP}, H_{pair}, and $(-\omega j_x)$ representing single-particle, pairing, and the cranking terms, respectively, one is able to express[23] the matrix elements of $H^{\omega}_{\text{soluble}}$ exactly with the help of simple analytical formulas. Consequently, the physical quantities of interest like $E=E(\omega)$ or $I=I(\omega)$ can also be calculated exactly.

A great advantage of the soluble model consists in the fact that also the most frequently used *approximations*, such as, for example, Hartree-Fock-Bogolyubov cranking, particle number projection, or random-phase-approximation (RPA) techniques lead to analytical expressions for the quantities of interest. Therefore the quality of various approximate methods can be straightforwardly tested relying totally on the analytical results. Such a detailed study has been recently completed for the HFBC, RPA, and PNP approximations, and thus here it will be sufficient to summarize the relevant final results.

The HFBC approach often provides a "reasonably" good approximation to the exact energy and spin expressions, for rotational frequencies which do not exceed certain critical value, $\omega=\omega_{\text{crit}}$. For $\omega>\omega_{\text{crit}}$ the approximation is generally poor, the HFBC solution coinciding with the so-called "trivial" or "unpaired" solution. Applying the PNP technique improves the agreement with the exact result considerably, especially for rotational frequencies close to ω_{crit} (cf., e.g., Fig. 8 of Ref. 24) and generally for $\omega>\omega_{\text{crit}}$. The nontrivial HFBC solution (for $\omega<\omega_{\text{crit}}$) is said to describe the "static" pairing correlations. The difference between, say, energy vs ω curves calculated exactly and with the help of the simple HFBC is believed to result mainly from the neglect of the effect of "dynamical" nature often referred to as "pairing fluctuations" or "dynamical pairing vibrations."

As mentioned above, there are two commonly used ways of improving the approximation (over the HFBC approach). In the PNP improvement evidently not only the static but also significant amount of dynamical pairing correlations is effectively taken into account since the final PNP result approximates the exact one very well (cf. discussion in Ref. 24). A formally nonequivalent way of improving the approximation (over the HFBC approach) is provided by the RPA treatment which approximates the exact analytical result with the quality comparable to that provided by PNP (cf., e.g., Fig. 1 in Ref. 25).

Let us emphasize that both discussed methods, although nonequivalent formally, provide similar improvements over the simple HFBC approximation, both reproducing the exact result for the yrast E vs ω dependences comparatively well. One may therefore expect that the bulk of the "extra" (over HFBC) pairing correlations is accounted for, although perhaps to a different extent, by both approximations. These extra correlations amount to $(6-8)\hbar$ in the I vs ω comparison of Fig. 4, and this brings the realistic theoretical results closer to the presently known data on ^{152}Dy. [The reader is referred to Ref. 25 for extensive discussion of the pairing vibration problem in rotating nuclei together with the higher-order effects treated in terms of the nuclear field theory (NFT); an independent study in this direction can be also found in Ref. 26.]

Another study performed recently[21] with the help of a soluble model sheds some light on the problem of "unusually" small deviations of I vs ω dependence from the linear one. Analysis of the pairing vibration in a rotating harmonic oscillator by making use of the RPA shows that the solutions depend on the rotational frequency in a characteristic way, namely, via parameter

$$q \sim \omega/\beta \ , \tag{15}$$

where β represents the nuclear elongation. The latter relation demonstrates the property of the so-called frequency-deformation scaling: the ω dependence of, e.g., $E(\omega)$, angular momentum alignment, or other derived quantities is *weaker for the well-deformed* nucleus as compared to the moderately deformed one.

In "realistic" potentials the above scaling property is more difficult to demonstrate analytically but numerical calculations confirm the similar trend. It takes, roughly speaking, more rotation (higher ω) for a superdeformed as compared to normal nucleus to undergo similar

rotation-induced changes.

Summarizing this part of the discussion let us stress the following.

(a) The existence of pairing correlations (which go beyond the part described in terms of the independent quasiparticle approximation $\equiv$ HFBC) is responsible for lowering the I vs ω dependence in ^{152}Dy by an approximately ω-independent amount of typically $(6-8)\hbar$.

(b) The spin dependence of the superdeformed equilibrium deformation in ^{152}Dy turns out to be very insignificant.

(c) The relatively weak dependence of E or I vs ω, as compared to the analogous quantities known from the normal deformed minima in many nuclei (also the triaxial minima in ^{152}Dy itself) can be viewed as a result of both the particularly ω-stable shell structure at the superdeformation and the deformation scaling mechanism as studied in Ref. 21.

IV. PROBLEMS OF POPULATION AND DEPOPULATION RELATED TO THE SUPERDEFORMED BANDS

Since the high-spin states are populated in heavy-ion collisions which lead in general to highly excited nuclear configurations the description of thermal excitations in the population process becomes inevitable. On the other hand, depopulation of the band at its lowest spin limit involves most likely the effect of pairing which again needs to be taken into account.

A. Population and thermal excitations

Let us begin by recalling the shape coexistence picture of the zero temperature limit (Fig. 1). It shows that, in principle, one should expect many competing local minima produced by quantum (shell) effects. "Heating up" a nucleus is known to result in washing the shell effects out. Thus, for each individual minimum one should expect a shape transition out of it to occur, formally at various "critical" temperatures $T_c(i)$ different for various $i=1,2,\ldots,$ minima. (One possible way of defining T_c is to relate it to the temperature at which the separating potential barrier vanishes in some area of the deformation space.) Typical examples are provided by most often studied prolate-to-oblate shape transitions in the so-called good rotor nuclei.[27] Here we will be particularly interested in transitions related to superdeformed states.

In statistical physics an analog of those transitions is provided by phase transitions in macroscopic objects. The analogy, for temperatures considered in this article lies not so much in dramatic differences between the states of nuclear matter at various equilibrium deformations but rather in the fact that for temperatures close to T_c the fluctuations (in nuclear case—shape fluctuations) are expected to be particularly large. (Discussion of some general aspects of stability loss at $T\sim T_c$ in statistically describable objects can be found in, e.g., Ref. 28.)

For the superdeformed minimum in ^{152}Dy the critical temperature, $T_c(\text{superdef})\sim 700$ keV over a broad spin range. While the superdeformed barriers on the free-energy landscapes vanish at this temperature, the numerical value of T_c as defined above has more formal rather than practical meaning since the shape fluctuations are probably large already for $T<T_c$. Our experimental knowledge about those fluctuations is too limited at the moment to allow for restrictive testing of the theories at this point. In the following we rather concentrate on the simplest consequences of our microscopic calculations of the free energy, illustrated in Sec. II, and their possible qualitative tests.

Our starting point is the observation that a nucleus produced at certain initial excitation energy, E_i^*, and spin I_i, must preserve both these quantities until an emission of, e.g., a quantum γ, a particle, etc., takes place. At typical excitation energies, after subtracting the rotational energy, *a significant part of what remains is the deformation energy.* Consider, for instance, a typical $A\sim 150$ nucleus where the fission barrier at spins $I\sim(10-20)\hbar$ amounts to ~ 25 MeV. Let us denote the rotational energy in the initial state by $E_i(\text{rot})$. At $E_i^*-E_i(\text{rot})\approx 20$ MeV, there will be areas in the deformation space where the full available excitation will be equal to deformation energy (temperature equal zero) and those where it may be totally gone into the thermal excitation $T\sim\sqrt{20/a}>1000$ keV [for an order of magnitude estimate here it will be sufficient to set $a\approx(A/8)$].

Thus when calculating the deformation related properties at the experimentally encountered situation, i.e., with the total excitation energy $E^*=\text{const}$, the free-energy representation in the usual form of F vs deformation at constant temperature is not of much help. [Let us note that despite this, the free-energy representation is still instructive when, for instance, the overall variation of the deformation energy can be considered weak over large areas of the deformation space and the constant E^* or constant T representations are nearly equivalent (cf. Sec. II, Fig. 3)]. Consequently we will need to reformulate the problem. We chose the reasoning very much in line with the early proposition of Moretto.[29]

Let us assume that the probability of finding the system at the point (E^*,I,β) can be expressed in terms of the corresponding nuclear level densities, ρ_I, by

$$P(E^*,I,\beta)dv\sim\sum_{e_n\le E^*}\rho_I(E^*-e_n)\rho_n(\beta,e_n)dv\ , \quad (16)$$

where e_n denotes the energy of a collective (oscillatory) motion in a state $|n\rangle$ and $p_n(\beta,e_n)$ is the related deformation-probability distribution. Let us recall that β stands for the deformation variables (β_2,γ) and dv is the corresponding volume element in the deformation space. Replacing the probabilities $p_n(\beta,e_n)$ by their quasiclassical limits and the summation in (16) by integration over e leads[29] to the following approximate result:

$$P(E^*,I,\beta)dv\sim\rho_I[U(I,T,\beta)]T(I,\beta)dv\ , \quad (17)$$

where $T(I,\beta)$ denotes the local nuclear temperature at deformation β. Here the Fermi gas formula[30] for ρ_I will be adopted:

$$\rho_I(U)=\frac{2I+1}{12}\left[\frac{\pi^2}{6}g_0\right]^{1/2}\left[\frac{\hbar^2}{2J(\beta)}\right]^{3/2}U(I,T,\beta)^{-2}$$
$$\times\exp\left\{2\left[\frac{\pi^2}{6}g_0U(I,T,\beta)\right]^{1/2}\right\}, \quad (18)$$

where g_0 represents the proton- and neutron-related single-particle level densities at the Fermi energies, and $J(\beta)$ is the corresponding (rigid rotor) moment of inertia. Result (17) shows that apart from a preexponential temperature dependence, the high-lying coherent (oscillatory) excitations do not modify the "primary" relation

$$P(E^*,I,\beta)\sim\rho_I[U(I,T,\beta)] . \quad (19)$$

In the following we limit ourselves to a qualitative discussion related to the above proportionality (quantitative results will be published elsewhere). It is important to remember that the nuclear level density not only determines the deformation probability distributions but also the population probability; for instance, assuming the giant-dipole type deexcitation as a dominating electromagnetic decay-feeding mode at high excitations leads to the following integrated decay transition probability from a state with I_i to I_f:

$$T_{\rm GDR}(E1;U_i)\sim\int_0^{U_i}\rho_{I_f}(U)/\rho_{I_i}(U_i)f_{\rm GDR}(U_i-U)(U_i-U)^4dU . \quad (20)$$

It will be instructive at this point to recall how the mechanism of disappearance of the shell effects (in particular, also the relative elevation of the deformation energy at various deformation points) influences the level densities and thus the population probabilities when temperature increases. Let us first combine relations (2, 8, and 9) which give:

$$R^{\omega}(\text{def},T)=E^{\omega=0}_{\rm macro}(\text{def})+\left[\sum_\nu e^{\omega=0}_\nu(\text{def})-\sum_\nu{}' \tilde n^{\omega=0}_\nu(\text{def})e^{\omega=0}_\nu(\text{def})\right]$$
$$+\left[\sum_\nu e^{\omega}_\nu(\text{def})-\sum_\nu e^{\omega=0}_\nu(\text{def})\right]+\left[\sum_\nu{}' n^{\omega}_\nu(\text{def},T)e^{\omega}_\nu(\text{def})-\sum_\nu{}' n^{\omega}_\nu(\text{def},T=0)e^{\omega}_\nu(\text{def})\right], \quad (21)$$

where $\sum_\nu$ extends over all the (lowest) occupied levels and $\sum'_\nu$ extends in principle to infinity (in practice the occupation coefficients assume very small values for energies extending sufficiently far above the Fermi levels and the summations stay always within finite limits). The first term within large square brackets in Eq. (21) stands for the $E^{\omega=0}_{\rm micro}$(def) of Eq. (2). The Strutinsky's occupation coefficients, $\tilde n^{\omega}_\nu$(def), can be calculated analytically, (cf., e.g., Ref. 15).

Taking into account that $n^{\omega}_\nu(\text{def},T=0)$ represents 1, for $e^{\omega}_\nu<\lambda=$ Fermi level, and 0 otherwise, implies that

$$\sum_\nu e^{\omega}_\nu(\text{def})-\sum_\nu{}' n^{\omega}_\nu(\text{def},T=0)e^{\omega}_\nu(\text{def})=0$$

and we obtain

$$R^{\omega}(\text{def},T)=E^{\omega=0}_{\rm macro}(\text{def})+\left[\sum_\nu{}' n^{\omega}_\nu(\text{def},\ T)e^{\omega}_\nu(\text{def})-\sum_\nu{}' \tilde n^{\omega=0}_\nu(\text{def})e^{\omega=0}_\nu(\text{def})\right] . \quad (22)$$

Equation (22) can be rewritten as follows:

$$R^{\omega}(\text{def},T)=E^{\omega=0}_{\rm macro}(\text{def})+\left[\sum_\nu{}' n^{\omega}_\nu(\text{def},T)e^{\omega}_\nu(\text{def})-\sum_\nu{}' n^{\omega=0}_\nu(\text{def},T)e^{\omega=0}_\nu(\text{def})\right]$$
$$+\left\{\sum_\nu{}'[n^{\omega=0}_\nu(\text{def},T)-\tilde n^{\omega=0}_\nu(\text{def})]e^{\omega=0}_\nu(\text{def})\right\} . \quad (23)$$

The first difference in the above relation represents the independent particle Routhian normalized to zero at $\omega=0$ and for the Woods-Saxon type potentials it can be approximated (see, e.g., Refs. 11 and 18 and references therein) by

$$-J(\text{def},T)\omega^2/2$$

where the moment of inertia J can be shown to satisfy for the increasing temperature (typically $T>0.5$ MeV)

$$J(\text{def},T)\to J_{\rm rigid}(\text{def},T=0)\equiv J_{\rm macro}(\text{def}) .$$

One can show further that the temperature-dependent occupation coefficients in the second bracket of Eq. (23) approach the corresponding Strutinsky distribution $\tilde n$, when temperature increases; it is then a decrease in this last term together with the above relation for the moments of inertia which, within Strutinsky method, gives rise to the disappearance of the shell effect in the total free Routhian. Increase in temperature eventually brings the complicated in general total Routhian landscapes into a smooth asymptotic form represented within the discussed method by

$$R^{\omega}(\text{def},T)\approx E^{\omega=0}_{\rm macro}(\text{def})-\tfrac{1}{2}J_{\rm macro}(\text{def})\omega^2 . \quad (24)$$

[We recall that within the temperature range considered here the T dependence in macroscopic energy and moment of inertia, Eq. (24), can be neglected.]

One can always transform the total free Routhian

$R^{\omega}(\text{def},T)$ to the energy representation as usual by

$$R^{\omega} \rightarrow E(I) = R + \omega I + TS \ . \tag{25}$$

Tabulating all the quantities of interest (R, S, U, etc.) in functions of ω, T, and deformations allows in particular to express the energy as $E = E(I,T,\beta)$. For each I and deformation point β, the condition $E(I,T,\beta) = E^* = \text{const}$ determines in particular the local temperature $T = T(I,\beta)$, and thus also the local $U = U(I,T,\beta)$. It should be emphasized that the discussed algorithm automatically takes into account the shape changes induced by increasing temperature in particular when calculating $U(I,T,\beta)$. Numerically solving the equation

$$E(I,T,\beta) = E^* \tag{26}$$

for various excitation energies we thus obtain the corresponding overall U and T dependence on deformation. This result can be used to evaluate the level densities [here we use Eq. (18) for the simple estimates] and possibly the deformation probabilities, via Eq. (17), or transition probabilities, via Eq. (20). (The latter two problems are left for the forthcoming publication.)

Results of the level density estimate are illustrated in Fig. 5 where curves corresponding to several excitation energies are shown. Note that to calculate transition probabilities the density formula must still be folded via integration in Eq. (20) with the giant dipole factor f_{GDR}. Nevertheless, the latter does not depend in any significant way on spin. Consequently, by comparing the estimates for the transition probability formula, Eq. (20), at increasing spin values ($I = 50$, 66, and 80 in Fig. 5) we are essentially testing the evolution in the exponentially varying density factor, the f_{GDR} being spin insensitive. Conversely, the dependence of the density factor (curves in Fig. 5) on spin imply the corresponding changes in the feeding distributions.

The results at $I = 50$ indicate a very strong (on the order of $\sim 10^3$) domination of the density factor at the normal deformation range over the super deformation range. At $I \sim 66$ the calculated level densities are comparable. This suggests, already in qualitative terms, a change in the side-feeding pattern between the two spin values. Thus at lower spins ($I \sim 50$) the population of normal-deformed states should dominate, while at $I \sim 60$ none of the two configurations would be strongly discriminated against the other. Indeed, the observed[3] feeding pattern indicates a strong tendency for the side feeding of the superdeformed band to decrease, or practically disappear, at spins as low as $I \sim 56$. The results of Fig. 5 suggest qualitative explanation of this pattern via level-density evolution with spin.

At still higher spin values, $I \sim 80$, the population of superdeformed states should be significantly favored (cf. right-hand-side frame in Fig. 5). However, the competition with the fission channel provides, in that spin range, an important counteracting factor which there may render a direct observation of the ^{152}Dy superdeformation very difficult (cf., nevertheless, comment in Sec. IV C).

Recently, an independent calculation[31] of the nuclear level densities using Nilsson-cranking model was performed. A comparison between the densities calculated here using the Woods-Saxon cranking model and those obtained within the Nilsson model made in a few deformation points indicates deviations only within a small nu-

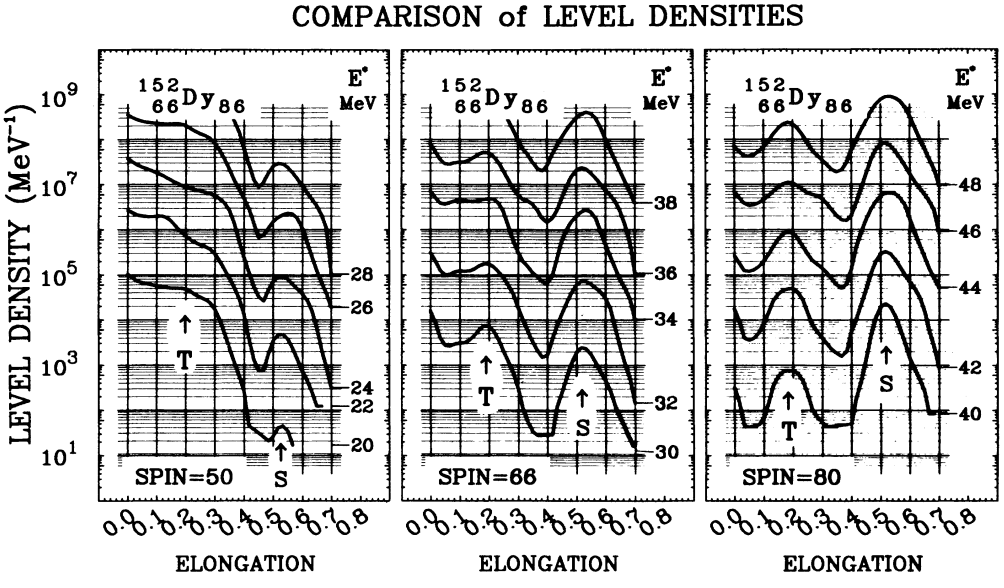

FIG. 5. Nuclear level densities calculated at the free-energy steepest descent trajectories on the (β,γ) plane of the standard quadrupole deformations, for the indicated total excitation energies E^*. The x coordinate is related to quadrupole elongation [positions of the arrows correspond to $\beta = 0.25$ (triaxial) and $\beta = 0.61$ (superdeformed)] minima. Level density parameter $a = A/8$; A is the mass number. Comparison with the results of the density calculations using independent method Ref. 31 has been possible in a few points at $I = 50$; the agreement is within a small numerical factor for the ^{152}Dy nucleus.

merical factor. A possible preexponential spin dependence of the density differing from that in Eq. (18), as discussed in Ref. 31, does not influence the conclusions of this article where we compare the densities at various deformation points for a given common value of spin.

Another problem to consider when looking for the optimum chances to observe the superdeformed states is related to the probability of "trapping" a nucleus in the corresponding minimum. Such a probability is believed to increase when the barrier between the super and the normal minimum increases. Results in Fig. 6 illustrate the dependence of the calculated barrier height (measured from the bottom of the superdeformed minimum) in function of both the spin and temperature. These results show, in quantitative terms, how the spin *increase* helps in building up the barrier thus counteracting the destructive influence of the increasing temperature. At spins $I \sim (70-80)$ the 1 MeV barrier, for instance, "survives" up to $T \sim (500-600)$ keV, while at $I \sim 50$ the corresponding limit would only be $T \sim 250$ keV.

The *most important* implication of the above results for optimizing population of the superdeformed configurations is to bring to the compound system the amount of angular momentum approaching the fission limit. Too low angular momentum in the system will produce both the unfavorable level-density conditions for populating superdeformed states, and nonoptimal trapping conditions because of the barrier behavior in function of temperature and spin.

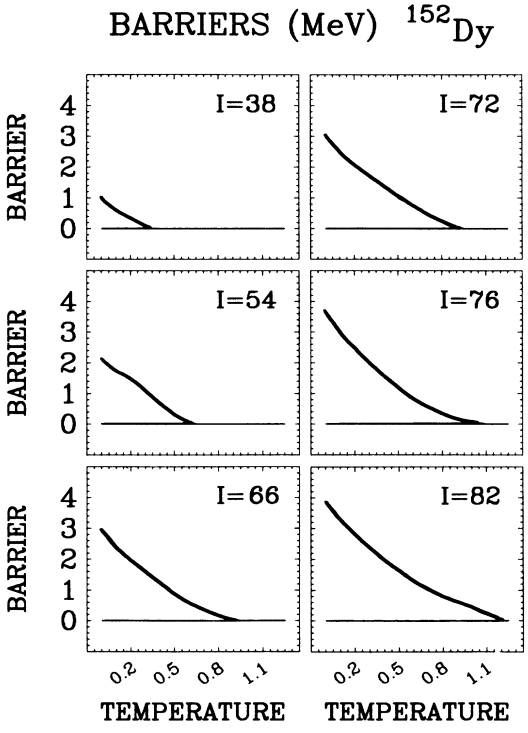

FIG. 6. The heights of the barriers separating the superdeformed and the triaxial minima on the free-energy surfaces as a function of temperature for the indicated spin values. Note that the barrier heights and thus the probability of trapping due to the potential barrier goes to zero at $T \sim 800$ keV, at $I \sim 60$.

While it is generally true that the probability of fission may quickly increase with spin, one may also expect that some (even small) probability of trapping the nuclei in superdeformed states will be sufficient for the observation by the contemporary 4π detection systems. The (HI,xn) reactions with largest possible x may offer here the most favorable conditions as it was the case in the recent ^{149}Gd study, Ref. 32.

B. Sudden depopulation of the superdeformed band at low spins and the effect of pairing

The fact that the superdeformed band has been observed down to $I \sim 24$ where its intensity suddenly disappears within three transitions can be understood in a simple way as indicative of disappearance of the potential barrier between the normal- and the super-deformed minima. Such a hypothesis contradicts the results of the Strutinsky-type calculations with the Nilsson model, Refs. 7 and 33, which show no indication of the barrier disappearance at the experimentally observed spin range. Present results, with the Woods-Saxon potential and the optimized classical energy of Møller and Nix[14] do not support the above picture indicating a very strong *decrease* of the barrier at $I \sim 20$. Thus, one may consider that there exists some "model dependent uncertainty" related to the decay out-of-band in the ^{152}Dy superdeformation case. However, even if the barriers do exist but are not extremely high over the spin range $I \sim (20-30)$ the chances for the nucleus to survive in the superdeformed minimum are not large because of pairing-related arguments and the barrier penetration mechanism. The problem of penetrating through potential barriers in the presence of pairing correlations has been considered by Bertch[34] and in the context of superdeformed nuclei, in Refs. 35, 36, and 20.

Summarizing the results of those studies brings us to the following argumentation. In the process of penetrating through the potential barrier the nuclear intrinsic configurations are often strongly rearranged. For instance, changing the nuclear shape from the lowest energy super-deformed state to the lowest energy normal-deformed state in ^{152}Dy is related to several (about 20) configuration rearrangements which in the mean-field approximation can be simply visualized as single-particle level crossings. The effective nuclear inertia related to such a deformation change can, under certain simplifying assumptions, be expressed by[20]

$$\bar{B} \sim \frac{g_\pi}{\Delta_\pi^2}\left[\frac{\Delta n}{\Delta\beta}\right]_\pi^2 + \frac{g_\nu}{\Delta_\nu^2}\left[\frac{\Delta n}{\Delta\beta}\right]_\nu^2, \tag{27}$$

where $(\Delta n/\Delta\beta)_{\pi,\nu}$ denotes the number of level crossings per deformation stretch $\Delta\beta$ for protons (π) or neutrons (ν), $\Delta_{\pi,\nu}$ denotes the average pairing gap and $g_{\pi,\nu}$ are the proportionality constants which can be further related to the single-particle level densities at the Fermi energies. The penetrability through the potential barrier at the energy E is, within the one-dimensional WKB approximation, given by

$$\text{penetrability} \sim \exp\left[-\frac{2}{\hbar}\int_{\beta_{\text{in}}}^{\beta_{\text{out}}}\sqrt{2\bar{B}[V(\beta)-E]}d\beta\right], \tag{28}$$

where $V(\beta)$ denotes the total nuclear potential in function of deformation and β refers in this case to a one-dimensional trajectory in the deformation space.

As it can be seen from the bottom part of Fig. 4, the average pairing correlations in the lowest energy superdeformed states are expected to increase significantly at decreasing rotational frequencies which correspond well to the discussed $I>20$ spin range. There, increasing in Δ_π^2 and Δ_ν^2 would cause an order of magnitude decrease in the average mass parameter $\bar{B}$, thus increasing significantly, via the exponential dependence in Eq. (28), the chances for an out-of-band penetration through the barrier. Therefore, more generally, even if the heights of the barriers at the low-spin range in superdeformed nuclei may be model uncertain to some extent, the pairing correlations at low rotational frequencies are likely to spur the out-of-band decay.

C. A comment on fission stability at high spins

From the discussion in Sec. IV A it becomes clear that the highest-spin limit would be optimal for the population of superdeformed states if not of the competition with fission. Here, however, the fast rotation factor may turn out to be crucial in stabilizing the superdeformed configurations. Indeed, in the highest-spin range considered ($I>50$) the average pairing factors Δ in Eq. (27) are expected to be very small (they should not be confused with the trivial $\Delta=0$ solutions of the simple HFBC method which fails at this frequency range). As the result, the effective inertia parameters in fast rotating rare-earth (RE) nuclei should become significantly larger than, say, in the low-spin (and excitation) states of the actinide. Therefore, the comparable fission barriers for a superdeformed fast rotating state in a RE nucleus and a fission isomer in the actinide range may result in much stronger high-spin RE stability against fission because of differences in pairing.

D. Remarks on the enhanced population of the lowest superdeformed bands

There is a possibility that the enhanced population of *the lowest* superdeformed band may be perhaps viewed as an experimental confirmation of the presence of the strong shell structure. Indeed, the branching ratio for feeding

$$\Gamma_{\text{feed}}(\text{lowest})/\Gamma_{\text{feed}}(\text{excited}) \sim [(E_\gamma+\Delta E)/E_\gamma]^{2\lambda+1}$$

favors the population of the lowest band with $\Delta E \sim 800$ keV $\sim \min(\Delta E_\pi, \Delta E_\nu)$, $\lambda=1$ or 2, and $E_\gamma \sim (2-3)$ MeV, typically, by a factor of 2–3. However, one should expect that in general the higher lying excited superdeformed bands should also be populated and indeed some presence of intensity related to quasicontinuum has been reported.

This problem may have a more intimate connection to the fission-gamma decay competition. It apparently cannot be excluded that the so-called second chance fission (fission from the superdeformed state after say one or two $\lambda=1$ gamma rays have been emitted) wins in competition with the next, possibly low energy γ transition. Such a mechanism would effectively decrease the chances to populate the excited superdeformed bands in a few steps of relatively low transition energies E_γ as compared to those of high E_γ leading directly to the neighborhood of the lowest or just to the lowest superdeformed band.

One should emphasize at this point that the reported intensity of $\sim 0.2\%$ for the states close to the top of the superdeformed band in ^{152}Dy is still 1–2 orders of magnitude higher as compared to the extrapolated[36] intensity pattern of the normal bands in, e.g., ^{160}Er, ^{168}Yb, and ^{162}Hf. Intensities of the discrete transitions in those nuclei are known up to $I\sim 40$ and thus the corresponding extrapolation (confirmed by the Monte Carlo simulation test, cf. Fig. 1 in Ref. 36) seems to be sufficiently certain. The second chance fission mechanism, possibly related, needs further investigation from both theoretical and experimental points of view.

V. SUMMARY AND CONCLUSIONS

Using well-established methods of nuclear structure (deformed mean field of the Woods-Saxon type, generalized Strutinsky method with elements of the statistical model approach, independent quasiparticle method) the superdeformation properties of ^{152}Dy have been studied. The results can be summarized as follows.

(a) A coexistence between the three experimentally well-established shape configurations (oblate, triaxial, and superdeformed) is well reproduced by the applied techniques. The spin gain (I vs ω) calculated at the two collective minima, viz. triaxial and superdeformed, reproduces well the characteristic $I(\omega)$ behavior known experimentally for the two collective bands only after applying the particle number projection technique in the treatment of pairing. The simple so-called Hartree-Fock-Bogolyubov cranking method overestimates the experimental results by typically $(6-8)\hbar$, an amount which does not depend very much on rotational frequency. A possible interpretation of this result in terms of dynamical pairing effects has been discussed on the basis of previously completed studies on the exactly soluble models. It is argued that the influence of the so-called rotation-deformation scaling mechanism is contributing to some peculiarities of ^{152}Dy behavior.

(b) Minimization of the total energy with respect to deformation gives the following result: The positions of superdeformed minima on the (β_2,γ) plane are practically spin independent; on the contrary, the triaxial ones evolve markedly with rotation.

(c) The almost linear I vs ω dependence in the superdeformed configuration is reproduced within only a small inaccuracy margin. Suggested mechanisms contributing here are the strong and relatively stable against rotation shell (gap) effects in both the neutron and proton systems. (One should stress that this property is related to a particular shell structure in ^{152}Dy, and possibly also some

other nuclei, rather than a general feature related to any superdeformed configuration.)

(d) Nuclear level density dependence on deformation at fixed total excitation energies and spin is calculated. These results are used to argue that at spins slightly in excess of $50\hbar$ and below, the side feeding of the ^{152}Dy superdeformed band should decrease fast with decreasing spin, in good qualitative agreement with what is observed.

(e) Depopulation of the superdeformed band at the low-spin limit (out-of-band escape), according to the present calculation, may be attributed to a significant lowering of the relevant potential barriers at spins approaching $I \sim 20$ range from above. Even if the calculated barrier heights are somewhat uncertain due to a possible model dependence, the influence of an increase in pairing on the barrier penetrability is expected to depopulate the band. Calculations predict a significant increase in both proton and neutron pairing correlations in the superdeformed ^{152}Dy minima at spins approaching $I \sim 20$ from above.

(f) Calculations predict also a "fourth" class of nuclear shapes (in addition to oblate, triaxial, and superdeformed). They posses quadrupole deformation $\beta_2 \sim 0.9$ (super-superdeformation), with a significant hexadecapole component, and are expected to compete with the usual superdeformed states very high in spin ($I \sim 80$). (More optimal cases for possible observation of those super-superdeformed states have been suggested in Ref. 20.)

ACKNOWLEDGMENTS

The Joint Institute for Heavy Ion Research has as member institutions the University of Tennessee, Vanderbilt University, and the Oak Ridge National Laboratory; it is supported by the members and by the Department of Energy through Contract No. DE-AS05-76ER0-4936 with the University of Tennessee. This work was supported in part by the Polish Ministry of Science and Education within the project CPBP 01.09 and by the Commemorative Association for the Japan World Exposition.

[1] J. Styczen, Y. Nagai, M. Piiparinen, A. Ercon, and P. Kleinheinz, Phys. Rev. Lett. **50**, 1752 (1983).

[2] B. M. Nyako, J. Simpson, P. J. Twin, D. Howe, P. D. Forsyth, and J. F. Sharpey-Schafer, Phys. Rev. Lett. **56**, 2680 (1986).

[3] P. J. Twin, B. M. Nyako, A. H. Nelson, J. Simpson, M. A. Bentley, H. W. Cranmer-Gordon, F. D. Forsyth, D. Howe, A. R. Mokhtar, J. D. Morrison, J. F. Sharpey-Schafer, and G. Sletten, Phys. Rev. Lett. **57**, 811 (1986).

[4] M. A. Bentley, G. C. Ball, H. W. Cranmer-Gordon, P. D. Forsyth, D. Howe, A. R. Mokhtar, J. D. Morrison, J. F. Sharpey-Schafer, P. J. Twin, B. Fant, C. A. Kalfas, A. M. Nelson, J. Simpson, and G. Sletten, Phys. Rev. Lett. **59**, 2141 (1987).

[5] T. Bengtsson, M. E. Faber, G. Leander, P. Moller, M. Ploszajczak, I. Ragnarsson, and S. Aberg, Phys. Scr. **24**, 200 (1981); C. G. Andersson, R. Bengtsson, T. Bengtsson, J. Krumlinde, G. Leander, K. Neergaard, P. Olanders, J. A. Pinston, I. Ragnarsson, Z. Szymanski, and S. Aberg, Phys. Scr. **24**, 266 (1981).

[6] Y. Schulz, J. P. Vivien, F. A. Beck, T. Byrski, C. Gehringer, J. C. Merdinger, J. Dudek, W. Nazarewicz, and Z. Szymanski, Phys. Rev. Lett. **48**, 1534 (1982).

[7] I. Ragnarsson and S. Aberg, Phys. Lett. B **180**, 191 (1986); T. Bengtsson and I. Ragnarsson, Nucl. Phys. A **436**, 14 (1985).

[8] H. Riezebos, A. Balanda, J. Dudek, J. van Klinken, W. Nazarewicz, Z. Sujkowski, and M. J. A. de Voigt, Phys. Lett. B **183**, 277 (1987).

[9] J. Dudek and W. Nazarewicz, Phys. Rev. C **31**, 298 (1985).

[10] P. Ring and P. Schück, *The Nuclear Many Body Problem* (Springer-Verlag, New York, 1980), cf. also references therein; M. de Voigt, J. Dudek, and Z. Szymanski, Rev. Mod. Phys. **43**, 949 (1983).

[11] A. V. Jgnatyuk, I. M. Mikhailov, L. H. Molina, R. G. Nazmitdinov, and K. Pomorski, Nucl. Phys. **A346**, 191 (1980).

[12] J. Dudek, in *Proceedings of the XXV International Winter Meeting on Nuclear Physics, Bormio, Italy, 1987,* edited by I. Iori (Ricerca Scientifica et Educazione Permanente, Milano, 1987).

[13] S. Cwiok, J. Dudek, W. Nazarewicz, J. Skalski, and T. Werner, Comput. Phys. Commun. **46**, 379 (1987), and references therein. For triaxial version of the potential see also, e.g., J. Dudek, *Proceedings of the XXV International Winter Meeting on Nuclear Physics,* Ref. 12, and references therein; J. Dudek, W. Nazarewicz, and N. Rowley, Phys. Rev. C **35**, 1489 (1987).

[14] P. Moller and J. R. Nix, Nucl. Phys. **A361**, 117 (1981); At. Data Nucl. Data Tables, **26**, 165 (1981).

[15] M. Bolsterli, F. O. Fiset, J. R. Nix, and J. L. Norton, Phys. Rev. C **5**, 1050 (1972).

[16] C. G. Anderson, S. E. Larsson, G. Leander, P. Moller, S. G. Nilsson, I. Ragnarsson, S. Aberg, R. Bengtsson, J. Dudek, B. Nerlo-Pomorska, K. Pomorski, and Z. Szymanski, Nucl. Phys. **A268**, 205 (1976).

[17] R. Bengtsson, J. Dudek, W. Nazarewicz, and P. Olanders, submitted to Phys. Scr.

[18] K. Neergaard, V. V. Pashkevich, and S. Frauendorf, Nucl. Phys. **A262**, 61 (1976); K. Neergaard, H. Toki, M. Ploszajczak, and A. Faessler, *ibid.* **A287**, 48 (1977); S. Cwiok, I. N. Mikhailov, and Ch. Briancon, Z. Phys. A **314**, 337 (1983).

[19] M. Diebel, K. Albrecht and R. W. Hasse, Nucl. Phys. **A355**, 66 (1981).

[20] J. Dudek, Proceedings of the International Conference on Nuclear Shapes, Crete, Greece, 1987.

[21] W. Nazarewicz, Z. Szymanski, and J. Dudek, Phys. Lett. B **196**, 404 (1987).

[22] J. Dudek, A. Majhofer, and J. Skalski, J. Phys. G **6**, 447 (1980).

[23] K. T. Hecht, Nucl. Phys. **63**, 177 (1965).

[24] W. Nazarewicz, J. Dudek, and Z. Szymanski, Nucl. Phys. **A436**, 139 (1985).

[25] D. Bes, R. A. Broglia, J. Dudek, W. Nazarewicz, and Z. Szymanski, submitted to Ann. Phys. (N.Y.).

[26] Y. R. Shimizu, E. Vigezzi, and R. A. Broglia, Phys. Lett. B **198**, 33 (1987); F. Barranco, M. Gallardo, and R. A. Broglia, *ibid.* **198**, 19 (1987).

[27] P. Ring, L. M. Robledo, J. L. Egido, and M. Faber, Nucl. Phys. **A419**, 261 (1984); A. Goodman, Phys. Rev. C (in press);

S. Levit and Y. Alhassid, Nucl. Phys. **A413**, 439 (1984); Y. Alhassid, J. Zingman, and S. Levit, *ibid.* **A469**, 205 (1987).
[28]H. B. Callen, *Thermodynamics* (Wiley, New York, 1961).
[29]L. Moretto, Nucl. Phys. **A182**, 641 (1972).
[30]A. Bohr and B. R. Mottelson, *Nuclear Structure* (Benjamin, New York, 1975) Vol. II.
[31]S. Aberg, in *Proceedings of the XXV International Winter Meeting on Nuclear Physics, Bormio, Italy, 1987,* edited by I. Iori (Ricerca Scientifica et Educazione Permanente, Milano, 1987); and (unpublished).
[32]B. Haas, P. Taras, S. Flibotte, F. Banville, J. Gascon, S. Cournoyer, S. Monaro, N. Nadon, D. Prevost, D. Thibault, J. K. Johansson, D. M. Tucker, J. C. Waddington, H. R. Andrews, G. C. Ball, D. Horn, D. C. Radford, D. Ward, C. St. Pierre, and J. Dudek, Phys. Rev. Lett. **60**, 503 (1988).
[33]I. Ragnarsson, T. Bengtsson, G. Leander, and S. Aberg, Nucl. Phys. **A347**, 287 (1980).
[34]G. Bertch, Phys. Lett. **B95**, 157 (1980).
[35]B. Herskind, B. Lauritzen, K. Schiffer, R. A. Broglia, F. Barranco, N. Gallardo, J. Dudek, and E. Vigezzi, Phys. Rev. Lett. **59**, 2416 (1987).
[36]B. Herskind and K. Schiffer, in *Superdeformed ^{152}Dy—Population and Decay*, Proceedings of the International School of Physics "Enrico Fermi," Course 36 CIII, Varenna, 1987, Italy, edited by P. Kienle, R. A. Ricci, and A. Rubino (Societa Italiana di Fisica, Bologna, 1987).

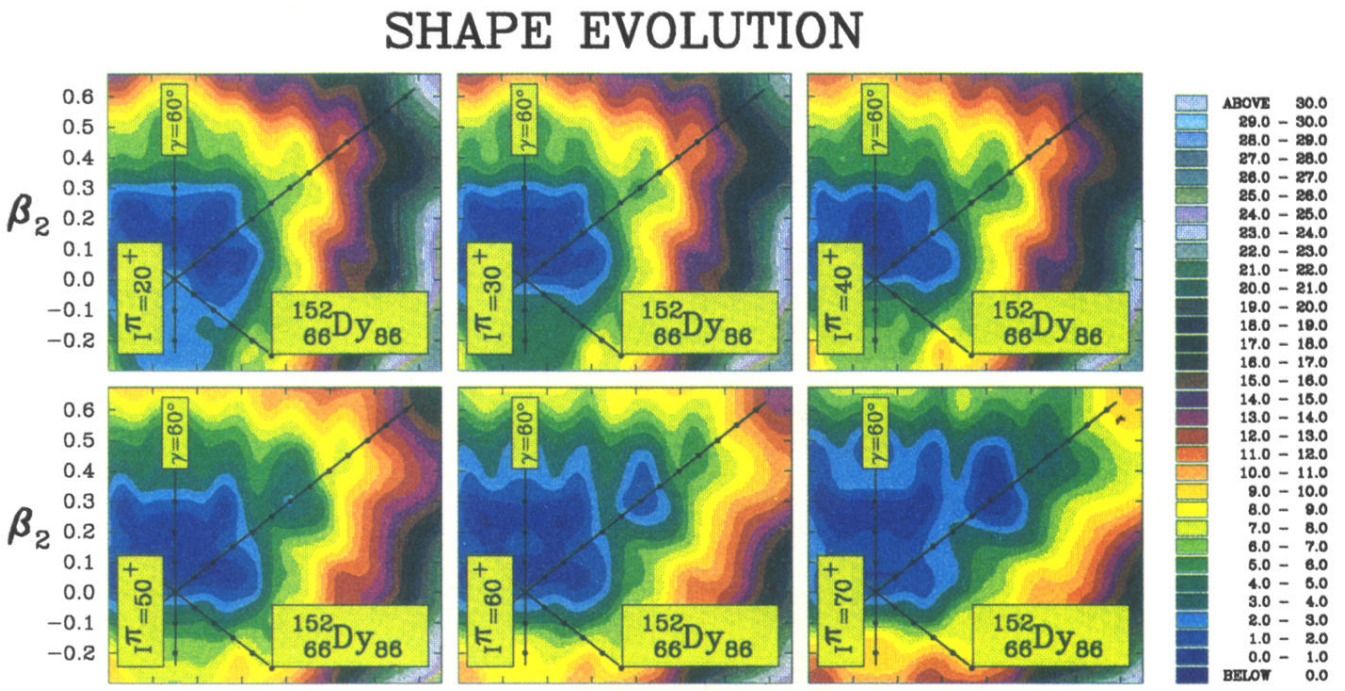

FIG. 1. The total energy surfaces in the (β_2,γ) plane with the $\beta_4=\beta_4(\beta_2,\gamma)$ optimized, as discussed in text. The convention related to the sign of the triaxiality parameter γ is as follows: $\gamma=60°$ corresponds to oblate shape noncollective rotation with spin parallel to the symmetry axis, $\gamma=0°$ (nearly diagonal axis) corresponds to collective rotation of the prolate deformed nucleus with the symmetry axis perpendicular to spin, etc. The lowest energy minima are marked with dark blue in the landscapes and the color scale defines the energy elevation (in MeV).

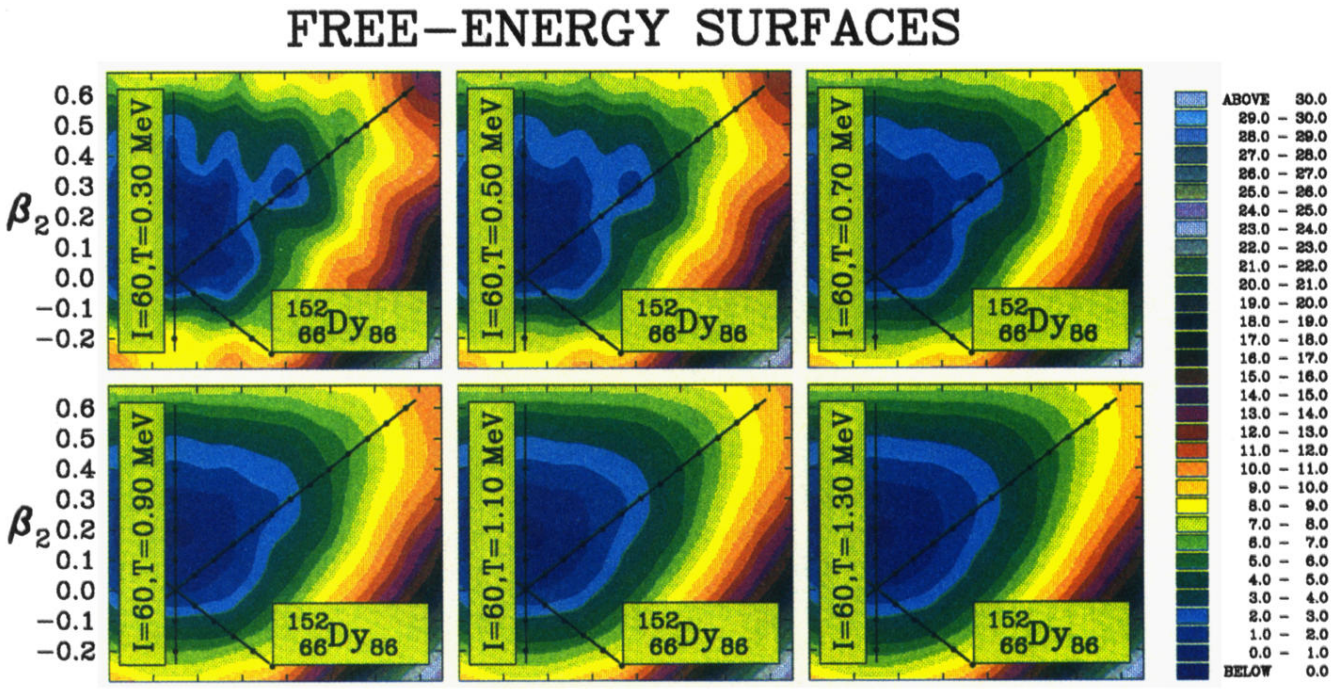

FIG. 2. The total free-energy surfaces calculated as discussed in text for $I=60$. Various frames correspond to increasing temperature. Note the early disappearance of the shell structure responsible for various coexisting minima already at $T\sim 800$ keV. The definition of the coordinate system is the same as in Fig. 1.

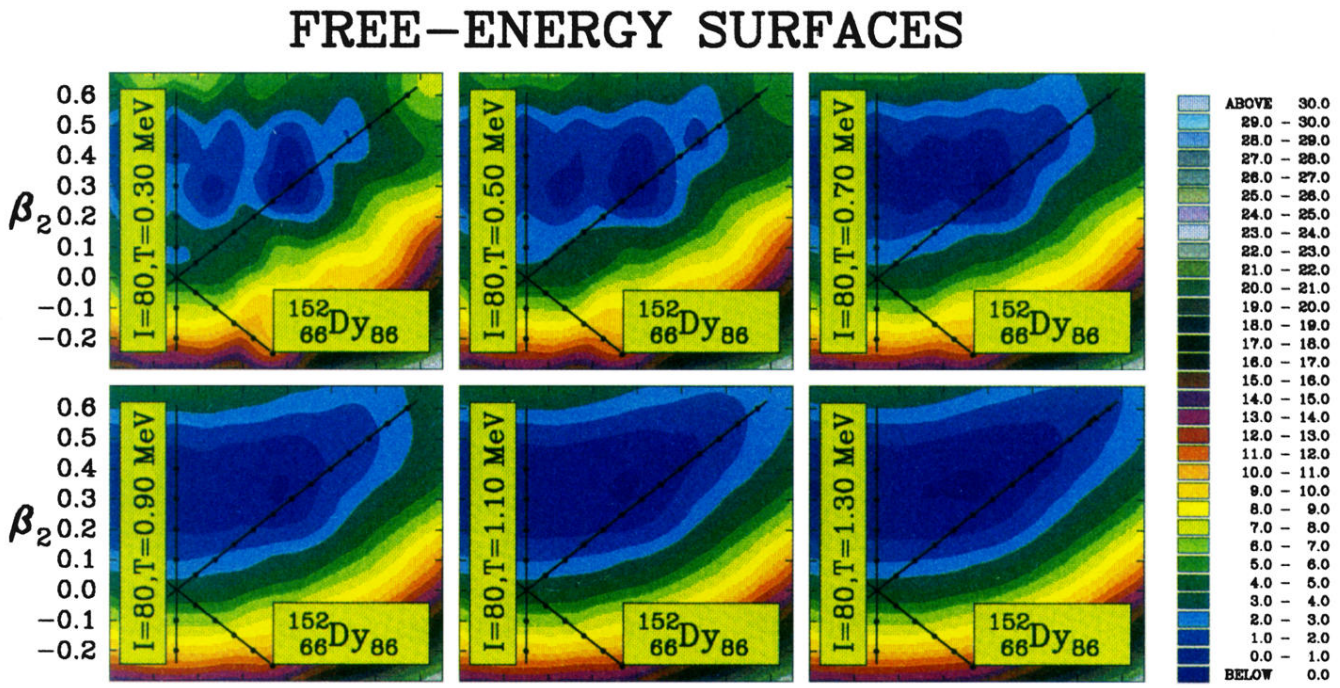

FIG. 3. Similar to Fig. 2 but at $I = 80$, i.e., close to the so-called Jacobi instability (for more details see captions to Figs. 1 and 2). Note that disappearance of the shell structure responsible for various minima affects the barrier height considerably.